Observation of Small Polaron and Acoustic Phonon Coupling in Ultrathin $La_{0.7}Sr_{0.3}MnO_3/SrTiO_3$ Structures

Bo Liu, Wei Niu, Xuezhong Ruan, Chunhui Zhu, Xuefeng Wang,* Liang He, Wenqing Liu, Edmond Turcu, Fengqiu Wang, Rong Zhang, and Yongbing Xu**

Understanding the underlying physics of interactions among various quasi-particles is a fundamental issue for the application of spintronics and photonics. Here the observation of a coupling between the small polarons in the nanoscale ultrathin $La_{0.7}Sr_{0.3}MnO_3$ (LSMO) films and the acoustic phonons in the $SrTiO_3$ (STO) substrate using ultrafast pump–probe spectroscopy has been reported. According to the temperature- and wavelength-dependent measurements, the amplitudes of the acoustic phonons are suppressed by tuning the small polarons absorption. This shows a coupled relationship between the acoustic phonons and the small polarons. At the probe photon energy of 1.55 eV where the polaron absorption is dominant, the acoustic phonons become unobservable. Furthermore, by performing the pump fluence dependent measurements on the LSMO films with different thicknesses, smaller acoustic phonon amplitudes are found in the thinner film with stronger small polaron binding energy. Such a coupled nature can be utilized to manipulate the small polarons using the acoustic phonons or vice versa, which is of great importance in device applications of colossal magnetoresistance materials.

Understanding the mechanisms of how various quasi-particles in solid state interact with each other is a fundamental issue. Insights into in this area are greatly helpful for various applications such as optical manipulation of magnetism[1] and potential magnetic recording.[2,3] The colossal magnetoresistance (CMR) of manganite compounds provide an ideal platform for investigating this topic. In the hole-doped perovskite manganites such as $La_{1-x}Sr_xMnO_3$ and $La_{1-x}Ca_xMnO_3$, the ferromagnetism and the metallicity below the Curie temperature T_C are explained by the double-exchange mechanism, where the itinerant e_g electrons gain the kinetic energy. The kinetic energy is maximum when the core spins of the neighboring Mn 3d t_{2g} localized electrons are well aligned.[4–6] The relevance between ferromagnetism and metallicity reflects the coupled relationship between the spin and electron degrees of freedom.

Couplings between the electron and the lattice degrees of freedom in the CMR materials have also been demonstrated by previous results.[7–12] Above T_C, the high resistance arises from the partial localization of the e_g electrons trapped by lattice distortions due to the Jahn–Teller (JT) effect that takes place on the Mn^{3+} sites.[13] The relaxation of JT distortion and its self-trapping effect usually takes effect within several picoseconds after photoexcitation at high temperature.[14–16] Therefore, the combination of double exchange interaction and the JT polarons plays a crucial role in determining the magnetic and electrical properties of these manganites.

Besides the polarons, the coherent acoustic phonons are also a kind of quasi-particles, which are employed to describe the lattice deformation. Studies on the acoustic phonons in different materials, such as ferromagnetic metals,[17] semiconductors[18] and their hetero-structures,[19] have been reported. The coupling between the acoustic phonons and the spins allows for fast control of the magnetization by injecting a high-amplitude acoustic wave packet into the magnetic layers. In manganites, to the best of our knowledge, the reported coherent acoustic phonons only focused on basic mechanical constants such as the sound velocity[20–24] in thick films (>75 nm). There are few reports on the coherent acoustic phonons in thin films of manganite oxides (<75 nm), let alone any couplings between the acoustic phonons and the other degrees of freedom such as spin, charge, and lattice. In this respect, studying the underlying correlations between the acoustic phonons and other quasiparticles is of great interest for both fundamental studies and

B. Liu, Dr. W. Niu, Dr. X. Ruan, Dr. C. Zhu, Prof. X. Wang, Prof. L. He, Prof. E. Turcu, Prof. F. Wang, Prof. R. Zhang, Prof. Y. Xu
Key Laboratory of Advanced Photonic and Electronic Materials
School of Electronic Science and Engineering
Nanjing University
Nanjing 210093, P.R. China
E-mail: xzruan@nju.edu.cn; xfwang@nju.edu.cn; ybxu@nju.edu.cn

Dr. W. Liu
Department of Electronic Engineering
Royal Holloway University of London
Egham TW20 0EX, UK

Prof. Y. Xu
Department of Electronic Engineering
York-Nanjing International Center of Spintronics (YNICS)
The University of York
York YO10 3DD, UK

The ORCID identification number(s) for the author(s) of this article can be found under https://doi.org/10.1002/pssr.201800657.

DOI: 10.1002/pssr.201800657

applications. This will provide new opportunities for manipulating the basic quasiparticles in electronic devices.

In recent years, due to the progress in femtosecond lasers and ultrafast spectroscopy techniques, the dynamic behavior of the electrons, spins, and lattice have been widely investigated in the time domain, showing various scattering channels on different time scales.[25–29] Since the interactions between different quasiparticles usually take effect on the time scale of picoseconds or nanoseconds, it is essential to study them with the ultrafast pump–probe method.

Here, we report a coupled relationship between the small polarons, i.e., quasiparticles which are formed by strong electron–phonon interactions, and the acoustic phonons in ultrathin LSMO films on the STO substrates. The absorption feature of the small polarons within a few picoseconds (ps) after photoexcitation was demonstrated by the transient reflectivity ($\Delta R/R$) curves. From the wavelength-dependent measurements, the amplitude of the acoustic phonons A_{osc} disappears at the probe photon energy of 1.55 eV that is the peak center of the small polaron absorption band. When the optical absorption of the small polarons was further tuned by changing the temperatures and the pump fluence, a corresponding modulation of A_{osc} was observed. The results demonstrate a coupled behavior between acoustic phonons and the polarons.

LSMO Thin Film Characterization: The epitaxial $La_{0.7}Sr_{0.3}MnO_3$ thin films were grown on (001)-oriented $SrTiO_3$ substrates by pulsed laser deposition and the growth details could be found elsewhere.[30,31] Two samples with the thickness of 40 and 3 unit cells (uc) were studied. The thickness and smoothness were controlled by reflection high energy electronic diffraction (RHEED). The Curie temperature (T_C) of the LSMO film of 40 uc (16 nm) is ≈334 K. In addition, the 3 uc (1.2 nm) LSMO layer exhibits paramagnetic insulator (PI) state.

Time-Resolved Reflectivity Spectra Results: **Figure 1**(a) illustrates the experimental configuration used in the measurements of transient reflectivity spectra (see Experimental Section). In order to generate a thermal stress as large as possible, we excite LSMO ultrathin films with 1.55 eV pump photon energy due to the higher absorption coefficient at this energy.[32] In this work, the excitation photon energy is 1.55 eV and the measurement is performed at room temperature unless otherwise specified.

Figure 2(a) shows a typical transient reflectivity trace $\Delta R/R$ of LSMO film with the thickness of 16 nm. The average pump fluence is 15 mJ cm^{-2}, corresponding to a density of excited electrons ≈10^{21} cm^{-3}. The probe photon energy in Figure 2(a) is 3.1 eV obtained from the second harmonic generation of the 1.55 eV laser output. The red oscillation component A_{osc} in the inset of Figure 2(a) is obtained by subtracting the background amplitude of $\Delta R/R$. The fast Fourier transform (FFT) results in Figure 2(c) show clearly two oscillation frequencies $f = 103$ GHz and $0.5f = 51$ GHz. These oscillations are described as the longitudinal coherent acoustic phonons. Their generation can be explained by the propagating strain pulse as discussed later or shown in Figure S1, Supporting Information.

In Figure 2(a) and (b), three characteristic responses are observed in different time windows from the temporal evolution of the $\Delta R/R$ profile. In Figure 2(b), a step-like instantaneous rise of $\Delta R/R$ occurs within 1 ps after the photoexcitation. This is followed by a second delayed step-like rising $\Delta R/R$ at $\Delta t = 10$ ps indicated by an arrow. The thermalization process between electrons and lattice systems reaches an equilibrium within the initial 10 ps, leading to a transient temperature increase of the sample due to the pump excitation. The $\Delta R/R$ decay time $\tau_d > 1$ ns arises either from the spin–orbit interaction[28,33] or the heat diffusion into the substrate or into the film itself.[27] The second step-like rise of $\Delta R/R$ (indicated by the arrow) is caused by the back-reflected pump beam from the bottom surface of the substrate. This is proven by the fact that the delay time $\Delta t = 10$ ps between the first and second step-like rise signal is equal to the reflected time Δt_r of the pump pulse by the back-surface of the substrate. Δt_r is calculated via $\Delta t_r = d_{sto}/v_{sto}$, where the substrate thickness $d_{sto} = 0.56$ mm and $v_{sto} = c/n_{sto}$. c is the speed of light and $n_{sto} = 2.64$[34] is the refractive index of substrate. Therefore, the Δt_r is varied as we change the wavelength of pump beam (see Figure S2, Supporting Information). Therefore, the actual physical time-zero is around $\Delta t = 10$ ps after the second pump excitation. The positive sign of $\Delta R/R$ at 3.1 eV probe photon energy is consistent with the well-established concept of spectral weight transfer, which is controlled by the spin correlations of t_{2g} spins.[14,29,35]

Optical Generated Coherent Acoustic Phonons: Now, we explain the generation of the acoustic phonons using the propagating strain pulse model.[36,37] In this model, the pump beam induces a transient thermal lattice expansion due to laser heating. This will generate a picosecond strain pulse that propagates from the LSMO film into the STO substrate. The interference between

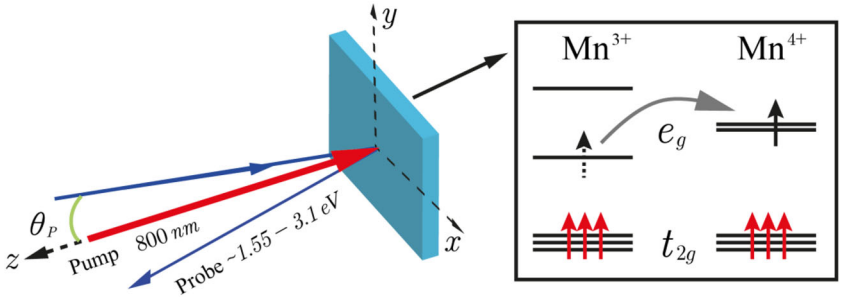

Figure 1. Experimental diagram for the ultrafast pump–probe reflectivity. θ_p is the angle between the sample normal and the incident direction of probe light. The right panel illustrates the intersite charge transfer of e_g electrons between the neighboring Mn ions excited by the photon energy of 1.55 eV.

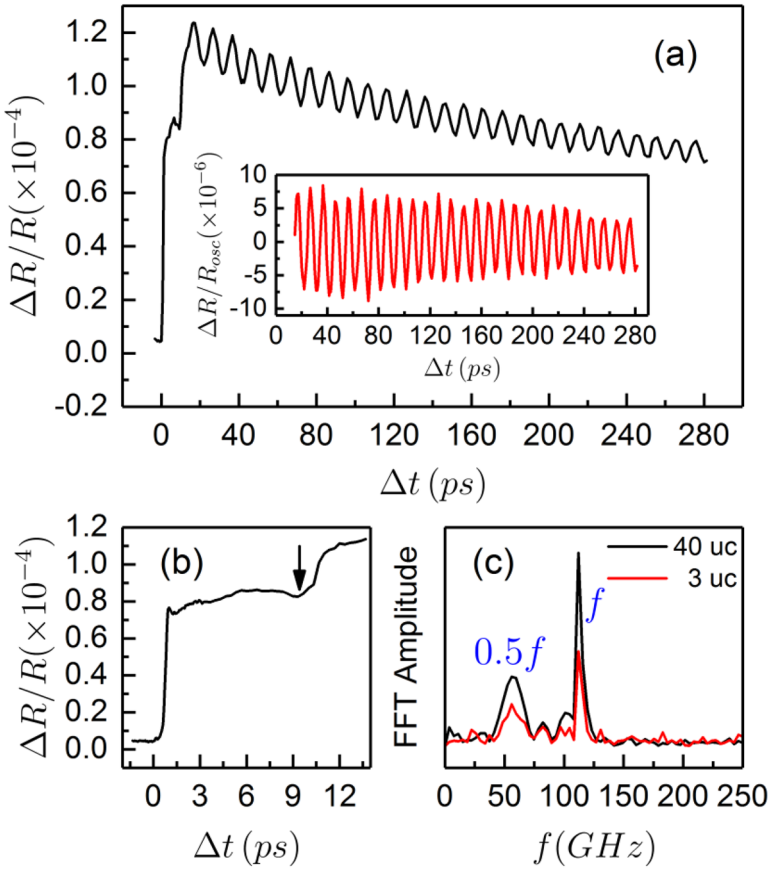

Figure 2. a) Transient reflectivity spectra of the LSMO film with a thickness of 40 unit cells. The pump and probe energies are 1.5 and 3 eV, respectively. The red oscillation component in the inset is obtained by subtracting the exponential-like decay background and is ascribed to longitudinal coherent acoustic phonon. b) Same spectra as in (a), but zoom-in on the first 14 ps of the photoinduced response. The triangle at around 10 ps represents the second time zero point between pump and probe pulse. c) FFT analysis of the oscillation part shown in (a). Here f denotes the acoustic phonon frequency detected by probe beam, while $0.5f$ arises from the interferences between pump beams and the propagating strain pulse.

probe beams reflected by the top surface of the sample and the propagating strain wave is responsible for the transient oscillations in $\Delta R/R$. These oscillations can be expressed as[20]

$$(\Delta R/R)_{\text{osc}} \propto A_{\text{osc}} e^{-t/\tau} \cos\left(\frac{4\pi n v t \cos\theta_{\text{p}}}{\lambda} + \phi\right) \quad (1)$$

Here, A, τ, and ϕ are the oscillation amplitude, the dephasing time, and the phase, respectively. n is the refractive index of substrate and v is the sound velocity of the acoustic wave. θ_{p} is the incident angle of the probe beam with respect to the normal direction of the sample. The oscillation components as a function of the incident angle and wavelength of the probe beam are well reproduced using Equation (1). This shows that the oscillations can be attributed to the coherent acoustic phonons. The detailed fitting procedure is shown in Figure S1, Supporting Information.

Correlation Between the Polarons and Acoustic Phonons: In **Figure 3**(b), the transient oscillations of 16 nm-thick LSMO film disappear at the probe photon energy of 1.55 eV. This phenomenon has never been reported previously in CMR materials, such as $LuMnO_3$,[20] $La_{0.67}Sr_{0.33}MnO_3$,[21] and $La_{1-x}Ca_xMnO_3$.[38] In their studies, the acoustic phonons can be observed at the probe photon energy of 1.55 eV. In Figure 3(a) and (b), a clear correlation between the acoustic phonons and the $\Delta R/R$ background is shown as we vary the probe photon energy. The amplitude of acoustic phonons decreases at 1.95 eV and totally disappears at 1.55 eV. Associated with this acoustic phonon variation, the $\Delta R/R$ profile also changes to the opposite sign. Thus, it is reasonable to infer that the disappearance of the transient oscillations may be caused by the appearance of the negative sign of $\Delta R/R$.

To verify this assumption, we need to first gain insight into the spectral feature of $\Delta R/R$, especially at 1.55 eV. It is because that the spectral weight transfers from high to low energies with decreasing temperatures (T) can lead to an optical conductivity spectrum change. This conductivity change can shape the profiles of $\Delta R/R$ at different photon energies in CMR materials.[11,14,33,39] The bottom panel of Figure 3(c) shows a simplified illustration of the differential optical conductivity $\Delta\sigma$ between 300 and 10 K. The data are obtained from Quijada et al.,[13] showing two broad band peaks centered around 1–2 eV and 3–5 eV, respectively. The values of $\Delta R/R$ measured at 14 and 341 ps are plotted in the upper panel of Figure 3(c). The

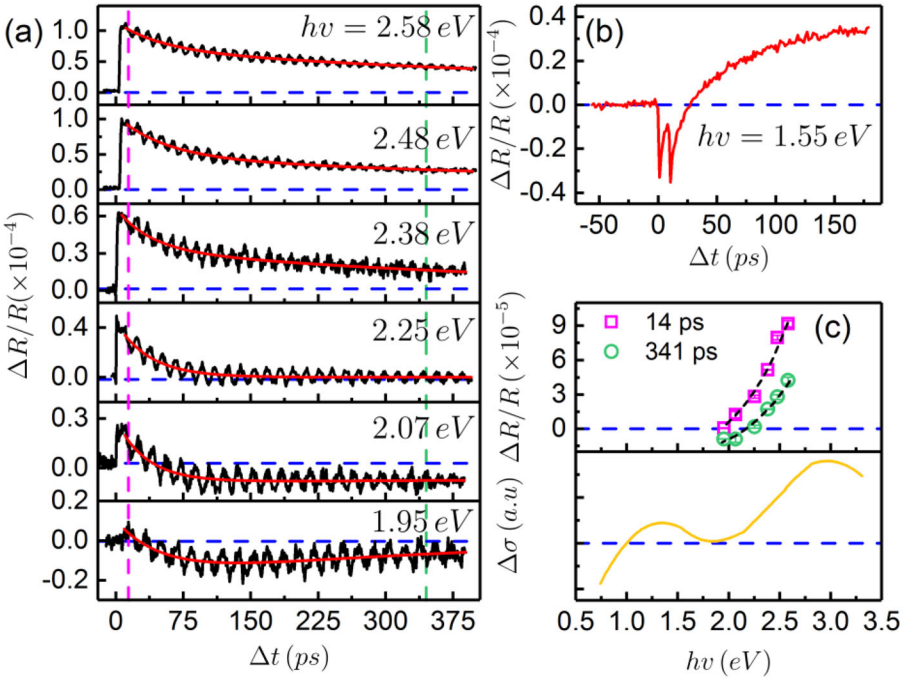

Figure 3. a) Transient reflectivity spectra of the 16 nm LSMO film at different probe photon energies. The red solid lines represent the fitting results by double-exponential decay functions. The two vertical dash lines mark the position of $\Delta t = 14$ and 341 ps, respectively. b) $\Delta R/R$ trace measured at 1.55 eV probe photon energy. c) Upper panel: The spectral dependence of $\Delta R/R$ measured at 14 and 341 ps after photo-excitation. The dash lines are used for guiding eyes. Bottom panel: Schematic diagram of the differential optical conductivity versus energy (simplified data redrawn from ref. [13]).

decreasing trends of both $\Delta R/R_{14\,ps}$ and $\Delta R/R_{341\,ps}$ as a function of probe energy are consistent with the variation $\Delta\sigma$ in the probe photon energy range of ≈1.95–2.58 eV as reported by Quijada et al.[13] This indicates that the $\Delta R/R$ profile in our measurement is dominated by the spectral weight transfer after photoexcitation. Such a consensus has been demonstrated by other optical conductivity measurements.[13,40,41] These reports have assigned the low-energy bands (1–2 eV) to the intersite optical transition of small polarons from the lower Jahn-Teller split e_g bands at a Mn^{3+} site to the higher e_g bands at a neighboring Mn^{4+} site. This hopping process is illustrated in the right panel of Figure 1(a). In our measurements, the probe photon energy of 1.55 eV lies in the high-energy tail of the polaron absorption bands. The negative sign of $\Delta R/R$ at initial time-delay exhibits a photoinduced transient increase of absorption. This is caused by the liberation of the small polarons due to the optical hopping. The negative sign in $\Delta R/R$ induced by the small polaron absorption has also been reported by other groups.[14,16,42] Since the second pump excitation at $\Delta t = 10$ ps, $\Delta R/R_{14\,ps}$ represents indeed the reflectivity dynamics at $\Delta t = 4$ ps. A larger reduction in $\Delta R/R_{14\,ps}$ compared to $\Delta R/R_{341\,ps}$ is seen in the upper panel of Figure 3(c) when the photon energy decreases to 1.95 eV. This is supported by the fact that the small polaron absorption usually happens within a few ps after the photo-excitation.

In order to reveal the effect of the small polarons on the acoustic phonons, we performed the temperature and pump-fluence dependent measurements on $\Delta R/R$ as shown in **Figure 4**. In Figure 4(a), the transient reflectivity traces at different temperatures is recorded. As the temperature T increases from 150 to 300 K, the values of $\Delta R/R$ within a few ps after photoexcitation decrease (indicated by the arrow). This decreasing trend originates from the enhancing small polaron absorption feature as the T increases. Since the generation of the acoustic phonons is due to the pump-induced lattice expansion, the amplitude of the acoustic phonons (A_{osc}) is proportional to change of lattice constants Δb. If we only take the lattice heating effect into consideration, according to the previous reports in $La_{1-x}Ca_xMnO_3$ ($x = 0.5,\ 0.58$)[38] and Pt/$SrTiO_3$,[43] the Δb is expected to increase with the increase of T. However, the A_{osc} in our measurements as shown in Figure 4(b) decreases with increasing T, showing that the small polarons can suppress the A_{osc}.

We also studied the pump fluence dependence of the A_{osc} at the probe photon energy of 3.1 eV. The raw data of $\Delta R/R$ for 16 and 1.2 nm samples under different pump fluences are shown in Figure S3, Supporting Information. In Figure 4(c) and (d), the values of $\Delta R/R_{14\,ps}$ and A_{osc} are plotted as a function of pump fluences. To compare the slopes, the amplitudes are normalized by dividing by their respective minimum values. For the 16 nm LSMO film in Figure 4(c), the slope of A_{osc} is about 1.6 times higher than that of $\Delta R/R_{14\,ps}$. While for the 1.2 nm sample in Figure 4(d), the slopes of A_{osc} and $\Delta R/R_{14\,ps}$ are almost the same. Such a behavior of the A_{osc} slope is because that small polaron absorption in the 1.2 nm film is more pronounced than that in 16 nm film.[44,45]

Based on the above temperature- and fluence-dependent measurements, we have demonstrated the existence of a coupling between the small polarons and the acoustic phonons. The decreasing A_{osc} from 2.58 to 1.95 eV shown in Figure 3(a) is because that the coupling strength increases as the probe photon

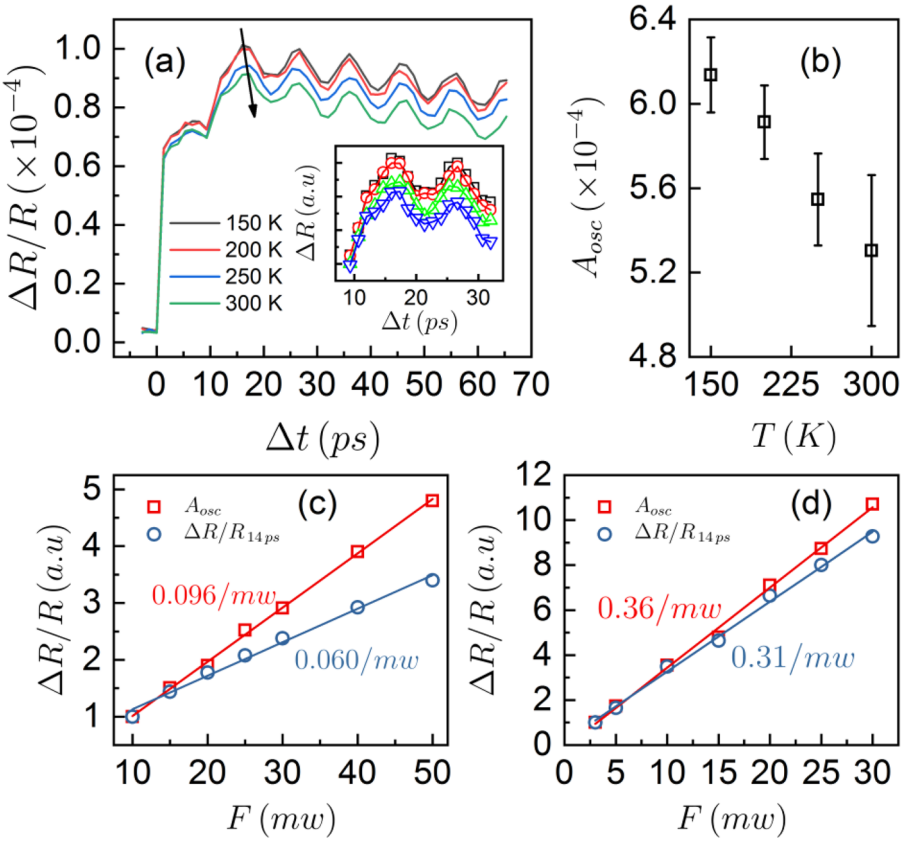

Figure 4. a) Transient reflectivity $\Delta R/R$ at temperature of 150, 200, 250, and 300 K. b) The amplitude of acoustic phonons A_{osc} as a function of temperatures from 150 to 300 K. The inset of (a) shows $\Delta R/R$ at a short time-window for clarity. The amplitude of $\Delta R/R$ at $\Delta t = 14$ ps and the A_{osc} as a function of pump fluence for the samples with thickness of 16 nm (c) and 1.2 nm (d). All the data are normalized by dividing the corresponding minimum values. The solid lines in (c) and (d) are the linear fitting lines. The pump and probe photon energies for both samples are 1.55 and 3.1 eV, respectively.

energy approaches small polaron absorption band center of 1.55 eV.

It is essential to discuss why previous reports[20,21,24] in CMR materials have observed the acoustic phonons in 1–2 eV. The main difference between our measurement and previous reports is the sample thicknesses. In our case, the film thicknesses are 16 and 1.2 nm, respectively. The thicknesses of the samples in previous studies (refs. [20,21,24]) were all larger than 75 nm. As demonstrated in perovskite manganites,[44,45] the polaron binding energy is stronger in the thinner films. Therefore, the polaron and acoustic phonon coupling in the thick films is not strong enough and the acoustic phonons are still observable.

In summary, by using the ultrafast pump–probe spectroscopy, we have discovered a coupling between small polarons and coherent acoustic phonons in ultrathin LSMO film deposited on STO substrate. From the spectral evolution of $\Delta R/R$, the A_{osc} is suppressed and even disappeared at the probe photon energy of 1.55 eV. The coupled relationship between them is demonstrated further by monitoring the variation of A_{osc} by tuning the absorption of small polarons via varying temperature and pump fluence. Our findings provide an opportunity for the manipulation of polarons and acoustic phonons through the coupled relationship between them.

Experimental Section

The pump-beam is nearly along the sample normal. The incident angle of the probe beam θ_p varied from ≈5° to 45° with respect to the normal direction of the sample plane. The pump pulse laser is generated by a Ti: sapphire regenerative amplifier with a pulse duration of 50 fs, a repetition rate of 1 KHz and a central photon energy of 1.55 eV. The photon energy of the probe beam is tuned by the optical parametric amplifier (OPA) from 1.95 and 2.58 eV. The pump beam is focused onto the sample by a 25 cm focal length lens to a spot diameter of 500 μm. The focused spot size of the probe beam is much smaller than that of the pump beam. Due to the delay stage, we can control the time arrival of the probe beam relative to the excitation of the pump beam and monitor the transient optical reflectivity of LSMO in time.

Supporting Information

Supporting Information is available from the Wiley Online Library or from the author.

Acknowledgments

This work is supported by National Key Research and Development Program of China (Grant No. 2016YFA0300803), the National Natural Science Foundation of China (Grant No. 61427812, 11774160,11574137, 11874203, 61822403, and U1732159) and and the Fundamental Research Funds for the Central Universities (Grant No. 021014380080). The authors also would like to thank the supports from the Collaborative Innovation Center of Solid State Lighting and Energy-saving Electronics and the Program for high-level Entrepreneurial and Innovative Talent Introduction, Jiangsu Province.

Conflict of Interest

The authors declare no conflict of interest.

Keywords

acoustic phonons, colossal magnetoresistance (CMR), perovskite manganites, small polarons

Received: December 10, 2018
Published online:

[1] J. Heidler, C. Piamonteze, R. V. Chopdekar, M. A. Uribe-Laverde, A. Alberca, M. Buzzi, A. Uldry, B. Delley, C. Bernhard, F. Nolting, *Phys. Rev. B* **2015**, *91*, 024406.
[2] E. Dagotto, T. Hotta, A. Moreo, *Phys. Rep*. **2001**, *344*, 1.
[3] F. Li, C. Song, B. Cui, J. Peng, Y. Gu, G. Wang, F. Pan, *Adv. Mater.* **2017**, *29*, 1604052.
[4] C. Zener, *Phys. Rev.* **1951**, *82*, 403.
[5] P. W. Anderson, H. Hasegawa, *Phys. Rev.* **1955**, *100*, 675.
[6] J. H. Park, E. Vescovo, H. J. Kim, C. Kwon, R. Ramesh, T. Venkatesan, *Nature* **1998**, *392*, 794.
[7] J. M. De Teresa, M. R. Ibarra, P. A. Algarabel, C. Ritter, C. Marquina, J. Blasco, J. García, A. del Moral, Z. Arnold, *Nature* **1997**, *386*, 256.
[8] C. S. Nelson, M. V. Zimmermann, Y. J. Kim, J. P. Hill, D. Gibbs, V. Kiryukhin, T. Y. Koo, S. W. Cheong, D. Casa, B. Keimer, Y. Tomioka, Y. Tokura, T. Gog, C. T. Venkataraman, *Phys. Rev. B* **2001**, *64*, 174405.
[9] V. Kiryukhin, T. Y. Koo, H. Ishibashi, J. P. Hill, S. W. Cheong, *Phys. Rev. B* **2003**, *67*, 064421.
[10] J. M. Caicedo, J. Fontcuberta, G. Herranz, *Phys. Rev. B* **2014**, *89*, 045121.
[11] Y. M. Sheu, S. A. Trugman, L. Yan, J. Qi, Q. X. Jia, A. J. Taylor, R. P. Prasankumar, *Phys. Rev. X* **2014**, *4*, 021001.
[12] S. Wall, D. Prabhakaran, A. T. Boothroyd, A. Cavalleri, *Phys. Rev. Lett.* **2009**, *103*, 097402.
[13] M. Quijada, J. Cerne, J. R. Simpson, H. D. Drew, K. H. Ahn, A. J. Millis, R. Shreekala, R. Ramesh, M. Rajeswari, T. Venkatesan, *Phys. Rev. B* **1998**, *58*, 16093.
[14] D. Talbayev, J. Lee, S. A. Trugman, C. L. Zhang, S. W. Cheong, R. D. Averitt, A. J. Taylor, R. P. Prasankumar, *Phys. Rev. B* **2015**, *91*, 064420.
[15] K. H. Wu, T. Y. Hsu, H. C. Shih, Y. J. Chen, C. W. Luo, T. M. Uen, J. Y. Lin, J. Y. Juang, T. Kobayashi, *J. Appl. Phys*. **2009**, *105*, 043901.
[16] H. Wang, D. Deng, Z. Zhang, K. Xu, Q. Pan, X. Lin, L. Yan, S. Cao, Z. Cheng, Z. Jin, G. Ma, *Phys. Status Solidi RRL* **2016**, *10*, 558.
[17] J.-W. Kim, J.-Y. Bigot, *Phys. Rev. B* **2017**, *95*, 144422.
[18] J. V. Jäger, A. V. Scherbakov, B. A. Glavin, A. S. Salasyuk, R. P. Campion, A. W. Rushforth, D. R. Yakovlev, A. V. Akimov, M. Bayer, *Phys. Rev. B* **2015**, *92*, 020404.
[19] A. V. Scherbakov, A. S. Salasyuk, A. V. Akimov, X. Liu, M. Bombeck, C. Brüggemann, D. R. Yakovlev, V. F. Sapega, J. K. Furdyna, M. Bayer, *Phys. Rev. Lett*. **2010**, *105*, 117204.
[20] D. Lim, R. D. Averitt, J. Demsar, A. J. Taylor, N. Hur, S. W. Cheong, *Appl. Phys. Lett*. **2003**, *83*, 4800.
[21] Y. H. Ren, M. Trigo, R. Merlin, V. Adyam, Q. Li, *Appl. Phys. Lett*. **2007**, *90*, 251918.
[22] I. Bozovic, M. Schneider, Y. Xu, R. Sobolewski, Y. H. Ren, G. Lüpke, J. Demsar, A. J. Taylor, M. Onellion, *Phys. Rev. B* **2004**, *69*, 132503.
[23] W. Li, B. He, C. Zhang, S. Liu, X. Liu, S. Middey, J. Chakhalian, X. Wang, M. Xiao, *Appl. Phys. Lett*. **2016**, *108*, 132601.
[24] Y. Ren, G. Lüpke, Y. Hu, Q. Li, C. S. Hong, N. H. Hur, *Phys. Rev. B* **2006**, *74*, 012405.
[25] T. Mertelj, D. Mihailovic, Z. Jagličič, A. A. Bosak, O. Y. Gorbenko, A. R. Kaul, *Phys. Rev. B* **2003**, *68*, 125112.
[26] T. Li, A. Patz, L. Mouchliadis, J. Yan, T. A. Lograsso, I. E. Perakis, J. Wang, *Nature* **2013**, *496*, 69.
[27] J. Bielecki, R. Rauer, E. Zanghellini, R. Gunnarsson, K. Dorr, L. Borjesson, *Phys. Rev. B* **2010**, *81*, 064434.
[28] A. I. Lobad, R. D. Averitt, C. Kwon, A. J. Taylor, *Appl. Phys. Lett*. **2000**, *77*, 4025.
[29] M. Rini, R. Tobey, N. Dean, J. Itatani, Y. Tomioka, Y. Tokura, R. W. Schoenlein, A. Cavalleri, *Nature* **2007**, *449*, 72.
[30] W. Niu, M. Gao, X. Wang, F. Song, J. Du, X. Wang, Y. Xu, R. Zhang, *Sci. Rep*. **2016**, *6*, 26081.
[31] W. Niu, X. Wang, M. Gao, Z. Xia, J. Du, Y. Nie, F. Song, Y. Xu, R. Zhang, *AIP Adv*. **2016**, *7*, 056404.
[32] J. Mistrík, T. Yamaguchi, M. Veis, E. Liskova, S. Visnovsky, M. Koubaa, A. M. Haghiri-Gosnet, P. Lecoeur, J. P. Renard, W. Prellier, B. Mercey, *J. Appl. Phys*. **2006**, *99*, 08Q317.
[33] T. Ogasawara, M. Matsubara, Y. Tomioka, M. Kuwata-Gonokami, H. Okamoto, Y. Tokura, *Phys. Rev. B* **2003**, *68*, 180407.
[34] M. Cardona, *Phys. Rev.* **1965**, *140*, A651.
[35] R. Rauer, M. Rubhausen, K. Dorr, *Phys. Rev. B* **2006**, *73*, 092402.
[36] C. Thomsen, H. T. Grahn, H. J. Maris, J. Tauc, *Phys. Rev. B* **1986**, *34*, 4129.
[37] K. Ishioka, A. Rustagi, U. Höfer, H. Petek, C. J. Stanton, *Phys. Rev. B* **2017**, *95*, 035205.
[38] D. Lim, V. Thorsmølle, R. Averitt, Q. Jia, K. Ahn, M. Graf, S. Trugman, A. Taylor, *Phys. Rev. B* **2005**, *71*, 134403.
[39] A. I. Lobad, A. J. Taylor, C. Kwon, S. A. Trugman, T. R. Gosnell, *Chem. Phys*. **2000**, *251*, 227.
[40] N. N. Kovaleva, A. V. Boris, C. Bernhard, A. Kulakov, A. Pimenov, A. M. Balbashov, G. Khaliullin, B. Keimer, *Phys. Rev. Lett*. **2004**, *93*, 147204.
[41] S. G. Kaplan, M. Quijada, H. D. Drew, D. B. Tanner, G. C. Xiong, R. Ramesh, C. Kwon, T. Venkatesan, *Phys. Rev. Lett*. **1996**, *77*, 2081.
[42] Y. G. Zhao, J. J. Li, R. Shreekala, H. D. Drew, C. L. Chen, W. L. Cao, C. H. Lee, M. Rajeswari, S. B. Ogale, R. Ramesh, G. Baskaran, T. Venkatesan, *Phys. Rev. Lett*. **1998**, *81*, 1310.
[43] A. Nagakubo, A. Yamamoto, K. Tanigaki, H. Ogi, N. Nakamura, M. Hirao, *Jpn. J. Appl. Phys*. **2012**, *51*, 07GA09.
[44] H. L. Liu, M. X. Kuo, J. L. Her, K. S. Lu, S. M. Weng, L. M. Wang, S. L. Cheng, J. G. Lin, *J. Appl. Phys*. **2005**, *97*, 113528.
[45] R. Prasad, H. K. Singh, M. P. Singh, W. Prellier, P. K. Siwach, A. Kaur, *J. Appl. Phys*. **2008**, *103*, 083906.

